ACS Photonics

Article

pubs.acs.org/journal/apchd5

Breaking the Challenge of Signal Integrity Using Time-Domain Spoof Surface Plasmon Polaritons

Hao Chi Zhang,[†] Tie Jun Cui,[*,†,‡] Qian Zhang,[†] Yifeng Fan,[†] and Xiaojian Fu[†]

[†]State Key Laboratory of Millimeter Waves, Southeast University, Nanjing 210096, China

[‡]Cooperative Innovation Centre of Terahertz Science, No.4, Section 2, North Jianshe Road, Chengdu 610054, China

Supporting Information

ABSTRACT: In modern integrated circuits and wireless communication devices or systems, three key features need to be solved simultaneously to reach higher performance and more compact size: signal integrity, interference suppression, and miniaturization. However, the above-mentioned requests are almost contradictory using the traditional techniques. To overcome this challenge, here we propose time-domain spoof surface plasmon polaritons (SPPs) as the carrier of signals. By designing a special plasmonic waveguide constructed by printing two narrow corrugated metallic strips on the top and bottom surfaces of a dielectric substrate with mirror symmetry, we show that spoof SPPs are supported from very low frequency to the cutoff frequency with strong subwavelength effects, which can be converted to the time-domain SPPs. When two such plasmonic waveguides are tightly packed with deep-subwavelength separation, which commonly happens in integrated circuits and wireless communications due to limited space, we demonstrate theoretically and experimentally that SPP signals on such two plasmonic waveguides have better propagation performance and much less mutual coupling than the conventional signals on two traditional microstrip lines with the same size and separation. Hence the proposed method can achieve significant interference suppression in very compact space, providing a potential solution to break the challenge of signal integrity.

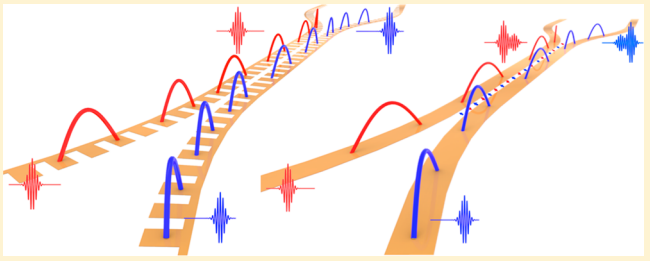

KEYWORDS: *surface plasmon polaritons, time domain, signal integrity, interference suppression*

Signal interference suppression and signal integrity are two of the most challenging topics in physics and electrical engineering. Especially, the rapid developments of super-large-scale integration of high-speed circuits and wireless communication systems/devices have brought forward higher requirements for signal interference suppression and signal integrity in the past decades.[1−3] Some special circuit strategies have been proposed to improve the signal quality, such as the equalization technique[4] and differential microstrip lines.[5] However, in the above techniques, additional areas of circuits and power consumptions are required, which make them rather difficult to utilize in high-frequency and/or high-speed circuits and systems. In fact, signal integrity, signal interference suppression, and miniaturization are three key features to be solved simultaneously to achieve higher performance and smaller size of complicated circuits and systems. But these factors are almost contradictory using the traditional transmission lines. To solve the challenges, we are forced to find new physics models beyond traditional transmission lines, and the surface plasmon polariton (SPP) approach is one of the possibilities due to its strong subwavelength effects.

At optical frequencies, because of the negative permittivity behavior of the metal and positive permittivity of the dielectric, SPPs are formed by the interaction between free electrons and the electromagnetic field[6,7] and propagate in parallel to the metal−dielectric interface with the exponential decay in the direction perpendicular to the interface. These special surface waves have inspired great interest and have been studied intensively during the past decades, owing to the extraordinary ability of field confinement[8] and potential applications in super-resolution imaging,[9,10] miniaturized sensors,[11] and photovoltaics.[12] Due to the unique properties of SPPs, optical circuits based on SPPs are generally recognized as one of the most promising avenues for further development, although some sophisticated theories still need to be established and validated.[13]

Even though SPPs have such excellent superiorities, they cannot be naturally achieved at low frequencies (i.e., microwave and terahertz) because metals show the characteristics of a perfectly electric conductor (PEC) rather than a plasmon with negative permittivity. To overcome this difficulty, the idea of constructing SPPs using metamaterials, so-called spoof SPPs or designer SPPs,[14] has been proposed.[15] Since spoof SPPs inherit the properties of SPPs and metamaterials, they can realize most of the unique features of optical SPPs, and the physical characteristics of spoof SPPs can be designed at will by tuning the geometrical parameters.[16−23] More recently, an ultrathin corrugated metallic strip structure[24] has been reported to realize conformal surface plasmons (CSPs), which are one of

Received: June 5, 2015
Published: August 7, 2015

DOI: 10.1021/acsphotonics.5b00316
ACS Photonics 2015, 2, 1333−1340

the most promising candidates for conformal circuits due to their flexibility and near-zero thickness. Based on an ultrathin corrugated metallic strip, an active spoof SPP device—the SPP amplifier—has been obtained at wideband microwave frequencies,[25] which can amplify the SPP waves by 20 dB, providing the foundation of potential spoof SPP integrated circuits and systems.

Here, we propose to solve the signal-integrity challenge using time-domain spoof SPPs as the carrier of signals in the microwave frequency range. We design a special plasmonic waveguide that is composed of two ultrathin corrugated metallic strips printed on the top and bottom surfaces of a dielectric substrate with mirror symmetry. Such a plasmonic waveguide is capable of supporting spoof SPPs from a very low frequency to a cutoff frequency, hence time-domain spoof SPPs. When SPP signals are propagating along two very closely packed plasmonic waveguides, as shown in Figure 1a, they

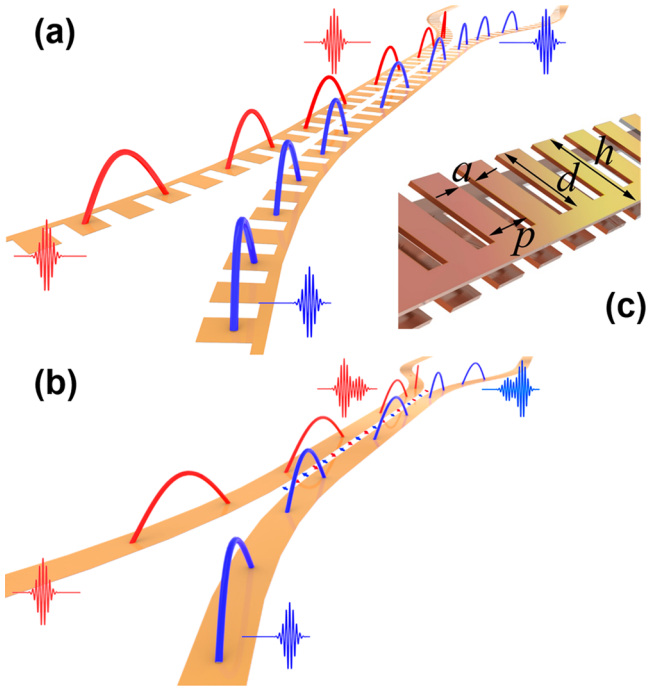

Figure 1. Two closely packed transmission lines of different types, which have different abilities to suppress interference. (a) Two closely packed spoof SPP waveguides, in which the interference is significantly suppressed. (b) Two closely packed microstrip lines, which have severe mutual interference. (c) Detailed structure of the SPP waveguide.

show excellent transmission performance and a powerful ability to suppress signal interference, which are verified by both numerical simulations and experiments. Possessing the features of strong field confinements, significant interference suppression in very compact space, and natural filtration, the proposed method may play an important role in realizing complicated SPP integrated circuits and systems.

The ultrathin conformal SPP structure is a big advance for microwave and terahertz SPP circuits due to its flexibility and broadband signal.[24] But this structure cannot naturally coalesce with conventional microwave circuits because of the single-line geometry. It was shown that the ultrathin corrugated metallic strip is able to confine the electromagnetic fields in two orthogonal directions and propagate the SPP waves with very low loss. However, the single-strip structure has two inevitable flaws in applications: (1) it is inconvenient to integrate with an active chip in the microwave frequency; (2) it cannot support low-frequency SPP waves, which leads to signal distortion when transmitting time-domain signals.

Different from optical systems, most modern electronic circuits require designers to integrate the digital part with the high-frequency part for the purpose of system stability. Hence the basic transmission lines must have the capabilities to support both low-frequency (e.g., 2.5 GHz clock signal in the digital module) and high-frequency (e.g., microwave and millimeter wave) signal transmissions. It is well known that most traditional transmission lines (e.g., microstrip lines) are based on double-conductor or multiconductor structures to support both low-frequency and high-frequency electromagnetic wave propagations, which are essential for time-domain signal transmissions. Hence, if we want to propose new types of transmission lines, they must have similar features to the traditional transmission lines to propagate both low-frequency and high-frequency signals. Strictly speaking, the concept of time-domain SPPs describes a series of SPP waveguides that can support continuous spectra of spoof SPPs from very low frequency to the cutoff frequency. Here, we adopt a special double-conductor plasmonic structure, which was initially designed to integrate with active chips.[25] However, in this design, spoof SPPs cannot be propagated at low frequencies (see Figure 5a in ref 25). To realize our goal, we have optimized the structure to support spoof SPPs from very low frequency (nearly zero) until the cutoff frequency.[28] The structure is composed of two corrugated metallic strips that are printed antisymmetrically on the top and bottom surfaces of a dielectric layer, as shown in Figure 1c. The double-strip plasmonic waveguide is constructed by arranging mirror duplicated unit cells periodically along the x-axis, in which the groove depth and groove width are denoted as d and a, and the strip width and thickness are h and t, respectively, with a period of p. Using a flexible dielectric substrate, this kind of plasmonic waveguide can also be designed to support conformal SPP modes, if required.

Figure 2a depicts the dispersion curves of the plasmonic waveguide with different groove depths d, in which the other geometrical parameters are chosen as a = 0.96 mm, h = 2.4 mm, t = 0.018 mm, and p = 2.4 mm, so that microwave SPPs are generated. Copper is selected as the metal, which can be regarded as a PEC in microwave frequencies, and the dielectric substrate is Rogers RT5880 with a dielectric constant of ε_r = 2.2, loss tangent tan δ = 0.0009, and thickness t_s = 0.508 mm. According to the previous theory and experience,[26,27] the ignored metal loss leads to a tiny blue shift of the dispersion spectrum but shows negligible impact on the shape of dispersion curve. This will simplify the eigenmode simulation carried out by the commercial software, CST Microwave Studio, and avoid the complex calculations. In Figure 2a, we clearly observe that the dispersion curves with different groove depths behave like natural SPPs at optical frequencies. All curves are deviating gradually from that of the microstrip line, from the traditional microwave transmission line, and further from the light line and then asymptotically approach different cutoff frequencies. More importantly, the performance of the slow wave becomes more and more striking as the groove depth d increases from 0.4 mm to 2.0 mm. Therefore, the dispersion curves are sufficiently sensitive to the change of groove depth d, which allows easy tuning of wave momentum,

DOI: 10.1021/acsphotonics.5b00316
ACS Photonics 2015, 2, 1333−1340

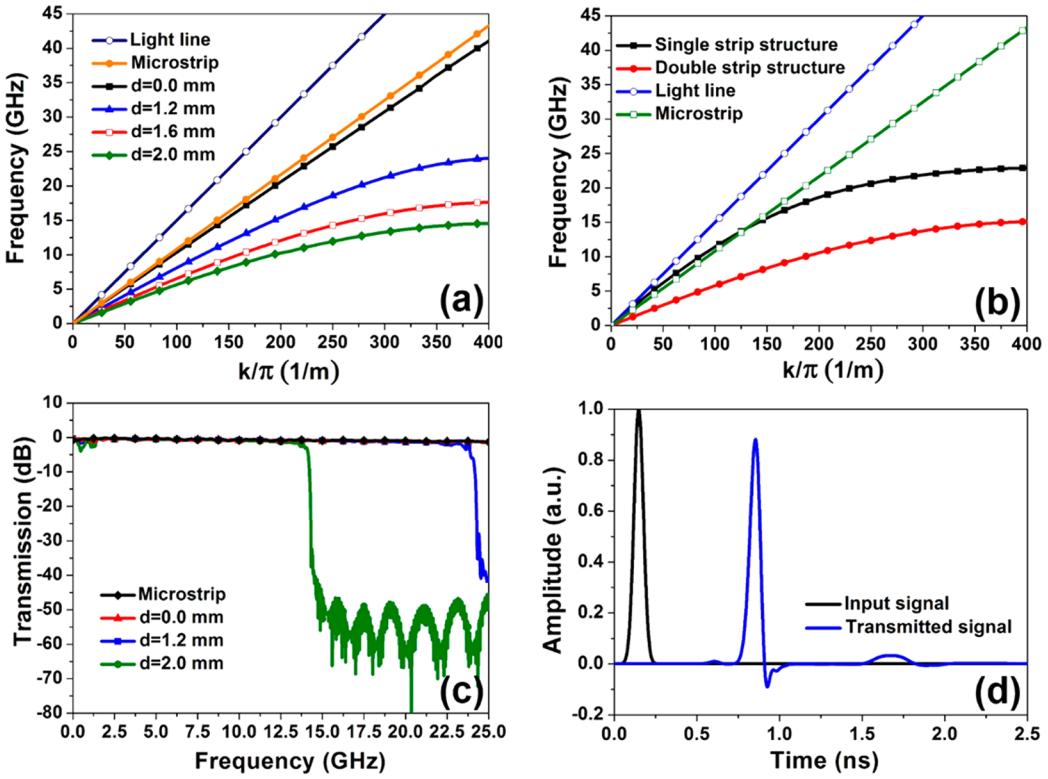

Figure 2. Simulated results of spoof SPP waveguides, in which the double-strip structure can support time-domain SPP signals. (a) Dispersion diagrams of the double-strip structure for different groove depths. (b) Dispersion diagrams for different kinds of waveguides. (c) Transmission spectra of the double-strip structures with different groove depths. (d) Time-domain SPP signal supported by the double-strip structure under the input of a Gaussian pulse with broadband signals from 0 to 12 GHz, in which a = 0.96 mm, h = 2.4 mm, d = 1.92 mm, and p = 2.4 mm.

making it possible to realize a smooth conversion between the SPP waves and conventional guided waves. For further investigation, we compare the dispersion characteristics of microstrip and single- and double-strip plasmonic waveguides under the same geometrical configuration, as illustrated in Figure 2b. We obviously notice that the dispersion curve of the double-strip structure deviates more significantly than that of the single-strip structure, which implies that the double strips can simultaneously confine the electromagnetic fields more tightly and enhance the fields more significantly around the structure.

One of the important features of the double-strip plasmonic waveguide is the guidance of low-frequency SPP waves, as demonstrated by the CST simulation results of transmission spectra in Figure 2c, in which the plasmonic waveguide has been matched to the microstrip line with 50 ohm impedance by using the gradient corrugation grooves.[28−30] From Figure 2c, we clearly observe that the transmission coefficients of the SPP waveguide are near unity (i.e., approximately 0 dB) from 0 to 12 GHz, which has equivalent transmission performance to the microstrip line that has been widely used in modern integrated circuits and wireless communication systems. This important feature implies that time-domain SPP signals that cover a large range of frequency spectra can be guided by the plasmonic waveguide. Figure 2d shows the transmitted time-domain SPP signal under the input of a Gaussian pulse with broadband signals from 0 to 12 GHz. We find that the transmitted SPP signal keeps very good waveform with tiny distortion, which is caused by the slight reflection and frequency dispersion.

Even though the frequency dispersion of the SPP waveguide produces a tiny distortion in the broadband signal, the natural filtration provides an additional advantage to integrate circuits. As shown in Figure 2a, each dispersion curve has a corresponding cutoff frequency. Once the operating frequency is higher than the cutoff frequency, the SPP waves cannot propagate through the plasmonic waveguide. This feature leads to a rapid decline in the transmission spectrum, as illustrated in Figure 2c, which looks like a filter.[31,32] This natural filtration provides a possibility to achieve miniaturizations of SPP circuits and systems by omitting the filter devices.

Owing to the interaction between two such corrugated metallic strips, the double-strip plasmonic waveguide demonstrates a more significant subwavelength effect and tighter field confinement than the single corrugated strip under the same geometrical configuration, which helps reduce mutual coupling and miniaturize the SPP devices. To further show the spoof SPP propagations on the plasmonic waveguide, we give the electric-field distributions of the SPP modes with different phase shifts, as depicted in Figure 3a. At low frequencies (smaller phase shifts), it is noted that the electromagnetic waves are mainly restricted between the two corrugated metallic strips, which is similar to the gap SPP mode in the coupling nanowire array.[33−36] As the frequency increases (i.e., the phase shift increases), we notice that the electric fields along the propagation direction are gradually enhanced, and the propagation mode gradually gets close to the SPP mode along the single corrugated metallic strip,[24] which confines the electric fields around the surface structure. The mode change can be reasonably explained by the enhanced confinement ability of the double-strip plasmonic waveguide with the increasing frequency.

DOI: 10.1021/acsphotonics.5b00316
ACS Photonics 2015, 2, 1333−1340

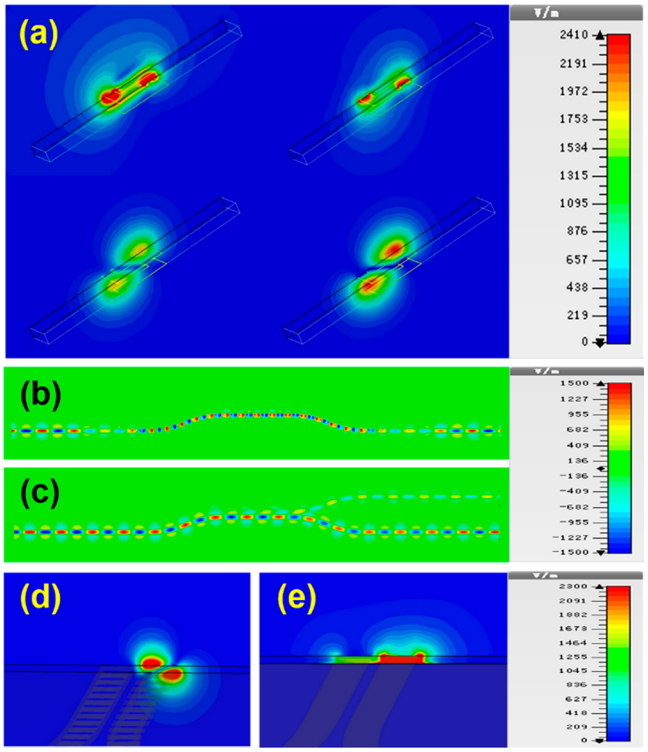

Figure 3. Simulated near electric-field distributions of the spoof SPP waveguide in different cases. In the right-hand coordinate system, the x- and z-axes are pointing to the directions of EM wave propagation and perpendicular to the structure surface, respectively. (a) Magnitude distributions of eigenmodes with different phase shifts. (b) Normal electric-field distribution of two closely packed SPP waveguides on the $x-y$ plane that is 1.0 mm above the plasmonic structure at 10 GHz. (c) Normal electric-field distribution of two closely packed microstrip lines on the same observation plane at 10 GHz. (d) Magnitude distributions of two closely packed SPP waveguides on the $y-z$ plane at 10 GHz. (e) Magnitude distributions of two closely packed microstrip lines on the $y-z$ plane at 10 GHz.

In integrated circuits and wireless communication devices (e.g., cell phones) or systems, it is usually requested that many transmission lines are packed in a compact space, and the strong mutual coupling results in a signal-integrity problem. Here we propose to solve the problem by using the novel plasmonic waveguide and time-domain SPP signals. Without the loss of generality, we consider two closely packed plasmonic waveguides (see Figure 1a) with a separation s = 0.8 mm, which is about 0.027 wavelengths at 10 GHz. For easy comparison with the conventional technique, we also consider two closely packed microstrip lines with the same geometry and separation (see Figure 1b). In fact, the physical insight for the plasmonic waveguide to reduce mutual coupling is the strong field confinement, which is also the major difference from the traditional microstrip line. This is confirmed by the numerical simulation results of electric fields under different states.

In Figure 3b and c, we present electric-field distributions on the plasmonic waveguides and microstrip lines on the $x-y$ plane, which is 1.0 mm above the structure surface at 11 GHz, in which the fields are excited from the left of the lower SPP waveguide or microstrip line. We clearly observe that the electric-field energy is tightly localized in a very small region near the plasmonic structure, leading to no interference (or mutual coupling) with the adjacent upper waveguide. In the microstrip lines, however, a remarkable interference is observed, resulting in significant coupling fields propagating on the upper microstrip line. We further notice that the propagating wavelength on the plasmonic waveguide is much smaller than that on the microstrip line, which is convenient to miniaturize the SPP devices and circuits. To show the detailed distributions around the gap area of two SPP waveguides or microstrip lines, we provide the magnitude distributions of electric fields on the $y-z$ plane, which is the central section of whole structure, as depicted in Figure 3d and e. Completely different from the single-strip structure,[28] we clearly see that the overlap of the electric fields on SPP waveguides is much more inconspicuous than those of microstrip lines, which reduces the mutual coupling (or crosstalk) significantly.

To study the crosstalk reduction quantitatively, we apply the coupling theory to evaluate the coupling coefficient. According to the coupled-mode theory,[37] the transmitted power ratio (T) and coupling power ratio (C) of the adjacent waveguide system can be expressed analytically as

$$\begin{cases} T = \cos^2(\kappa L)\mathrm{e}^{-2\alpha L} \\ C = \sin^2(\kappa L)\mathrm{e}^{-2\alpha L} \end{cases} \tag{1}$$

where L is the coupling length of the waveguide, α is the imaginary part of the propagation constant, and κ is the frequency-dependent coupling coefficient. For SPP modes, the coupling coefficient κ is written as[38]

$$\kappa = \frac{\omega\varepsilon_0}{4}\iint_{R^2}(n^2 - n_0^2)\left[\mathbf{E}_{1t}^{*}\cdot\mathbf{E}_{2t} + \frac{n_0^2}{n^2}\mathbf{E}_{1n}^{*}\cdot\mathbf{E}_{2n}\right]\mathrm{d}S \tag{2}$$

where n and n_0 are the refractive indices of the surrounding medium and the plasmonic waveguide, and $\mathbf{E}_{jt}$ and $\mathbf{E}_{jn}$ (j = 1, 2) are normalized transverse and longitudinal electric fields of plasmonic waveguide j, respectively. From eq 2, we observe that the coupling of adjacent plasmonic waveguides is caused by the overlap of electric fields in two such plasmonic waveguides. Hence it is possible to suppress the crosstalk of two adjacent SPP waveguides using the excellent feature of field confinement of SPPs.

Since the SPP field confinements can also lead to field enhancements, which may cause an adverse result, the design of an appropriate separation interval is very important. On the basis of this consideration, we made numerical simulations of the transmission and coupling ratios of the plasmonic waveguides and microstrip lines with different intervals, as illustrated in Figure 4a–d. From Figure 4a, the curves with intervals s = 0.4 mm have distinct dips in the transmission spectra of SPP waveguides, which suggests that the coupling in this case is potentiated by the field enhancement, and the behavior looks like a coupler rather than crosstalk suppression. The curve with interval s = 0.6 mm seems not to have a transmission dip, but in fact the dip caused by crosstalk meets the cutoff frequency, leading to a clearly different cutoff frequency. As the interval s increases from 0.8 mm to 2 mm, the transmission spectra do not exhibit noteworthy changes, which implies that the crosstalk is kept on a very low level in the passband (Figure 4c). For traditional microstrip lines, however, the transmission performance becomes worse and the crosstalk becomes more significant monotonically as the interval s decreases, as shown in Figure 4b and d.

In eq 2, we note that the coupling coefficient κ is a function of the propagation constant. In traditional microstrip lines, the coupling coefficient gradually increases as the propagation

DOI: 10.1021/acsphotonics.5b00316
ACS Photonics 2015, 2, 1333–1340

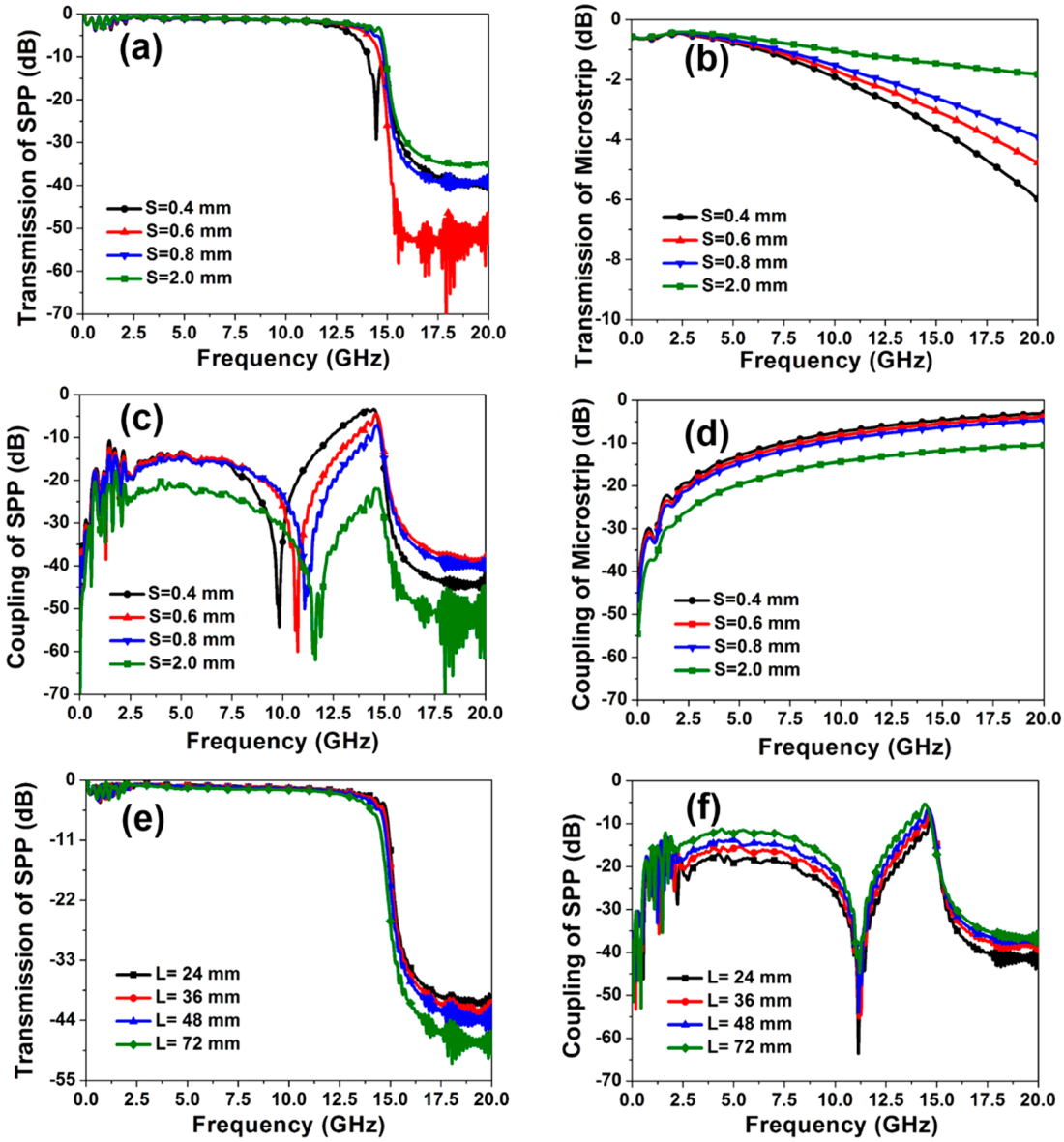

Figure 4. Simulated transmission and coupling coefficients in different cases. (a, b) The transmission coefficients of two closely packed SPP waveguides (a) and microstrip lines (b) with different separations. (c, d) The coupling of two closely packed SPP waveguides (c) and microstrip lines (d) with different separations. (e, f) Transmission (e) and coupling (f) coefficients of two closely packed SPP waveguides with different lengths.

constant increases (Figure 4d) due to the angular frequency factor. But in allusion to the SPP waveguides, the increase of propagation constant leads to tighter field confinement, which reduces the factor of field-overlapping contribution. Hence, different from that in microstrip lines, the crosstalk in SPP waveguides appears as undulation states in the frequency spectrum (Figure 4c).

The small coupling coefficient and low loss of SPPs lead to another beneficial feature, i.e., the transmission power ratio being nearly independent of the coupling length L. This feature can be proved by the minor approximations of eq 1, which are written as

$$\begin{cases} T = \cos^2(\kappa L)\mathrm{e}^{-2\alpha L} \approx 1 \\ C = \sin^2(\kappa L)\mathrm{e}^{-2\alpha L} \approx \kappa^2 L^2 \end{cases} \quad (3)$$

Equation 3 implies that the shape of the frequency spectrum is independent of the coupling length, which is confirmed by the numerical simulations shown in Figure 4e and f. This feature is very convenient in the engineering design, so that the influence of the coupling length does not have to be considered. The length-insensitive property of SPP waveguides is important evidence of the crosstalk suppression, which is completely different from that of the traditional microstrip lines.

To provide visual evidence, the time-domain SPP transmissions along the two SPP waveguides are simulated, which are excited by two Gaussian-pulse inputs with a time interval of 0.5 ns, as shown in Figure 5a. Here, with connections to potential applications, the input signal is chosen to have a bandwidth from 8 to 12 GHz, which is well known as the X band in the microwave frequency. From Figure 5a, we note that the existence of an adjacent plasmonic waveguide shows a negligible impact on the transmitted SPP signals, which have nearly no distortions after propagating through the SPP waveguide, illustrating excellent transmission performance without interference. As a comparison, the traditional trans-

DOI: 10.1021/acsphotonics.5b00316
ACS Photonics 2015, 2, 1333−1340

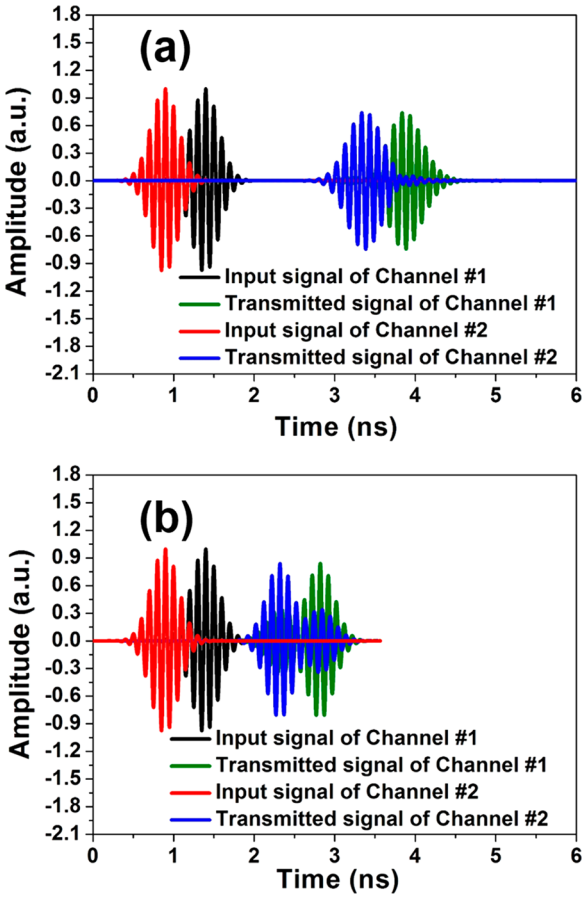

Figure 5. Simulated time-domain signal spectra of two closely packed transmission lines under the inputs of broadband Gaussian pulses (8–12 GHz) with a 0.5 ns time difference. (a) Two closely packed SPP waveguides. (b) Two closely packed microstrip lines. We remark that part of the transmitted signal curve of channel #1 is covered by the transmitted signal curve of channel #2.

mitted signals through the microstrip lines are demonstrated in Figure 5b, in which the transmitted signals are affected significantly, reaching glaring errors.

In the experiments, we fabricated two closely packed plasmonic waveguides, whose geometry parameters are the same as numerical simulations, based on the available printed circuit board technology, as shown in Figure 6a and c. Here, the separation between two waveguides is chosen as s = 0.8 mm (0.027 wavelength at 10 GHz). For comparison, we also fabricated two closely packed microstrip lines with the same geometries (Figure 6b and d). To conveniently measure the frequency spectra and near fields, we weld four standard SMA connectors to the four ports of the samples. Using the S-parameter measurement technique introduced below, we obtain the measured power transmission and coupling ratios from 0.03 to 20 GHz, and the results are presented in Figure 7a, which are in excellent agreement with the simulation results (Figure 4a). We clearly notice that the plasmonic waveguides and microstrip lines have nearly the same transmission performance below the cutoff frequency. However, the crosstalk or mutual coupling between the two plasmonic waveguides can be effectively suppressed. Compared with the microstrip lines, the crosstalk in the plasmonic waveguides is 10 dB lower on average from 6 to 15 GHz ($C_{SPPs} \leq C_{microstrip}/10$). Especially at the frequency of 11 GHz, the SPP crosstalk is decreased by 40 dB than the

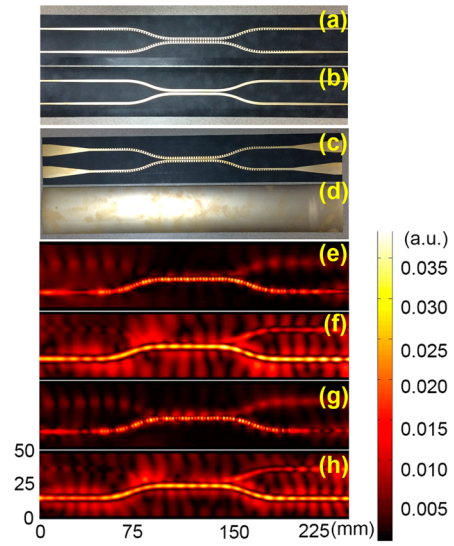

Figure 6. Fabricated samples and measured near-field results of the two closely packed transmission lines. (a, b) Top views of two closely packed SPP waveguides (a) and microstrip lines (b). (c, d) Bottom views of two closely packed SPP waveguides (c) and microstrip lines (d). (e, f) Measured near-field mapping results of the two closely packed SPP waveguides (e) and microstrip lines (f) at 11 GHz. (g, h) Measured near-field mapping results of the two closely packed SPP waveguides (g) and microstrip lines (h) at 12.5 GHz.

conventional way ($C_{SPPs} \approx C_{microstrip}/10\,000$). That is, there is a 4-order magnitude difference between the crosstalk of the plasmonic waveguide and microstrip, which can reduce the pressure of circuit designs and electromagnetic compatibility.

The measured time-domain transmitted SPP and microstrip signals are presented in Figure 7b and c. We observe that the transmitted SPP signals are nearly distortionless on passing through the plasmonic waveguide system due to the efficient interference suppression. However, the transmitted signals along the microstrip lines have significant distortions. To show the crosstalk reduction in a visual way, we also provide measurement results of near electric fields, as illustrated in Figure 6e–h. The near-field experiments are conducted by using homemade equipment (see below). We find that the spoof SPPs are propagating along their own waveguide with low loss with little mutual coupling to the other waveguide (Figure 6e and g). In contrast, the near-field distributions on the microstrip lines show longer wavelength and the more striking crosstalk (Figure 6f and h). Hence, the interference suppressions and subwavelength effects of time-domain SPP signals are demonstrated experimentally.

To solve the challenges of signal integrity in integrated circuits and complex devices or systems, we have proposed time-domain spoof SPPs as the carrier of signals, which are supported by a double-strip plasmonic waveguide. When two plasmonic waveguides are tightly packed with deep-subwavelength separation, we have demonstrated that the SPP signals have much less mutual coupling than conventional microstrip lines. The unique and beneficial features of strong field confinement, low crosstalk, and natural filtration of the plasmonic waveguides have been verified by both frequency-spectrum measurements and near-field mappings. As one of the most potential candidates for SPP integrated circuits and systems, the proposed method is very attractive for a variety of applications, such as high-speed circuits, parallel transmission

DOI: 10.1021/acsphotonics.5b00316
ACS Photonics 2015, 2, 1333–1340

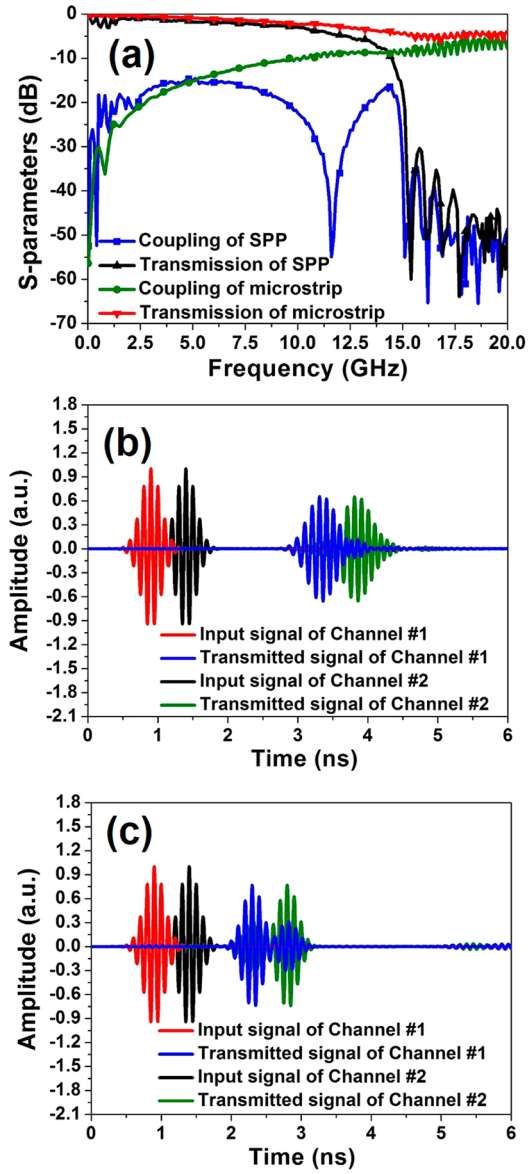

Figure 7. Measured result of two closely packed transmission lines. (a) Measured transmission and coupling coefficients of two closely packed SPP waveguides and microstrip lines. (b, c) Time-domain signal spectra of two closely packed SPP waveguides (b) and microstrip lines (c) under the inputs of broadband Gaussian pulses (8−12 GHz) with a 0.5 ns time difference. We remark that part of the transmitted signal curve of channel #2 is covered by the transmitted signal curve of channel #1.

systems, and conformal high-density integrated circuits. In addition, the method can be extended to higher frequencies (e.g., millimeter waves, terahertz waves, and far-infrared).

S-Parameter Measurements. The key apparatus we used in the *S*-parameter measurements is an Agilent vector network analyzer (VNA N5230C). However, it cannot measure the 4-port system directly. To solve this problem, we select one of the ports as the input port connected to port 1 of the VNA and measure the transmission coefficient (S_{21}) and reflection coefficients (S_{11}) of other ports successively. Note that the ports except the port connected to the VNA need to be loaded with a matching load over the measurements.

Near-Field Measurements. We conduct the near-field measurements using a homemade near-electric-field mapper, which is composed of a VNA (N5230C), a monopole antenna as the detector, and a planar platform that can move in the *x*- and *y*-directions automatically controlled by a stepper motor. The input port of the plasmonic waveguide is connected to port 1 of the VNA through the SMA to feed the energy, and the other port is connected to the matched load to eliminate reflections. To probe the vertical (z) components of the electric fields, the monopole antenna is fixed on top of the plasmonic waveguide around 1 mm and connected to port 2 of the VNA.

■ ASSOCIATED CONTENT

Supporting Information

The Supporting Information is available free of charge on the ACS Publications website at DOI: 10.1021/acsphotonics.5b00316.

Detailed descriptions of (1) smooth conversions between the plasmonic waveguide and microstrip line; (2) eigenmodes and excited modes of the plasmonic waveguide; (3) numerical results of two closely packed single-strip SPP waveguides; and (4) the effects of dielectric substrate thickness and fault tolerance (PDF)

■ AUTHOR INFORMATION

Corresponding Author

*E-mail: tjcui@seu.edu.cn.

Notes

The authors declare no competing financial interest.

■ ACKNOWLEDGMENTS

H.C.Z. and T.J.C. contributed equally to this work. This work was supported by the National Science Foundation of China (61171024, 61171026, 61138001, 61302018, and 61401089), National High Tech (863) Projects (2012AA030402 and 2011AA010202), and the 111 Project (111-2-05).

■ REFERENCES

(1) Johnson, H.; Graham, M. *High-Speed Signal Propagation: Advanced Black Magic*; Prentice Hall: Upper Saddle River, NJ, 2002.

(2) Caignet, F.; Bendhia, S. D.; Sicard, E. The Challenge of Signal Integrity in Deep-Submicrometer CMOS Technology. *Proc. IEEE* **2001**, *89*, 4.

(3) Fan, J.; Ye, X.; Kim, J.; Archambeault, B.; Orlandi, A. Signal Integrity Design for High-Speed Digital Circuits: Progress and Directions. *IEEE Trans. Electromagn. Compat.* **2010**, *52*, 392.

(4) Nazari, M. H.; Neyestanak, A. E. A 15-Gb/s 0.5-mW/Gbps two-tap DFE receiver with far-end crosstalk cancellation. *IEEE J. Solid-State Circuits* **2012**, *47*, 2420−2432.

(5) Hall, S. H.; Howard, L. H. *Advanced Signal Integrity for High-Speed Digital Designs*; Wiley-IEEE, 2009.

(6) Barnes, W. L.; Dereux, A.; Ebbesen, T. W. Surface plasmon subwavelength optics. *Nature* **2003**, *424*, 824−830.

(7) Shin, H.; Fan, S. H. All-Angle Negative Refraction for Surface Plasmon Waves Using a Metal-Dielectric-Metal Structure. *Phys. Rev. Lett.* **2006**, *96*, 073907.

(8) Yin, L. L.; Vlasko-Vlasov, V. K.; Pearson, J.; Hiller, J. M.; Hua, J.; Welp, U.; Brown, D. E.; Kimball, C. W. Subwavelength focusing and guiding of surface plasmons. *Nano Lett.* **2005**, *5*, 1399−1402.

(9) Jones, A. C.; Olmon, R. L.; Skrabalak, S. E.; Wiley, B. J.; Xia, Y. N.; Raschke, M. B. Mid-IR Plasmonics: Near-Field Imaging of Coherent Plasmon Modes of Silver Nanowires. *Nano Lett.* **2009**, *9*, 2553−2558.

(10) Fang, N.; Lee, H.; Sun, C.; Zhang, X. Sub-Diffraction-Limited Optical Imaging with a Silver Superlens. *Science* **2005**, *308*, 534−537.

DOI: 10.1021/acsphotonics.5b00316
ACS Photonics 2015, 2, 1333−1340

(11) Anker, J. N.; Hall, W. P.; Lyandres, O.; Shah, N. C.; Zhao, J.; Van Duyne, R. P. Biosensing with plasmonic nanosensors. *Nat. Mater.* **2008**, *7*, 442−453.
(12) Polman, A.; Atwater, H. A. Photonic design principles for ultrahigh-efficiency photovoltaics. *Nat. Mater.* **2012**, *11*, 174−177.
(13) Liu, N.; Wen, F.; Zhao, Y.; Wang, Y.; Nordlander, P.; Halas, N. J.; Alù, A. Individual Nanoantennas Loaded with Three-Dimensional Optical Nanocircuits. *Nano Lett.* **2013**, *13*, 142−147.
(14) Hibbins, A. P.; Evans, B. R.; Sambles, J. R. Experimental Verification of Designer Surface Plasmons. *Science* **2005**, *308*, 670−672.
(15) Pendry, J. B.; Martin-Moreno, L.; Garcia-Vidal, F. J. Mimicking surface plasmons with structured surfaces. *Science* **2004**, *305*, 847−848.
(16) Garcia-Vidal, F. J.; Martin-Meoreno, L.; Pendry, J. B. Surfaces with holes in them: new plasmonic metamaterials. *J. Opt. A: Pure Appl. Opt.* **2005**, *7*, S97.
(17) Williams, C. R.; Andrews, S. R.; Maier, S. A.; Fernandez-Dominguez, A. I.; Martin-Moreno, L.; Garcia-Vidal, F. J. Highly confined guiding of terahertz surface plasmon polaritons on structured metal surfaces. *Nat. Photonics* **2008**, *2*, 175−179.
(18) Maier, S. A.; Andrews, S. R.; Martin-Moreno, L.; Garcia-Vidal, F. J. Terahertz Surface Plasmon-Polariton Propagation and Focusing on Periodically Corrugated Metal Wires. *Phys. Rev. Lett.* **2006**, *97*, 176805.
(19) Atwater, H. A.; Polman, A. Plasmonics for improved photovoltaic devices. *Nat. Mater.* **2010**, *9*, 205−213.
(20) nAGPAL, P.; Lindquist, N. C.; Oh, S.-H.; Norris, D. J. Ultrasmooth Patterned Metals for Plasmonics and Metamaterials. *Science* **2009**, *325*, 594−597.
(21) Zhou, Y. J.; Jiang, Q.; Cui, T. J. Bidirectional bending splitter of designer surface plasmons. *Appl. Phys. Lett.* **2011**, *99*, 111904.
(22) Rivas, J. G. Terahertz: The art of confinement. *Nat. Photonics* **2008**, *2*, 137−138.
(23) Gan, Q.; Fu, Z.; Ding, Y. J.; Bartoli, F. J. Ultrawide-Bandwidth Slow-Light System Based on THz Plasmonic Graded Metallic Grating Structures. *Phys. Rev. Lett.* **2008**, *100*, 256803.
(24) Shen, X.; Cui, T. J.; Martin-Cano, D. F.; Garcia-Vidal, J. Conformal surface plasmons propagating on ultrathin and flexible films. *Proc. Natl. Acad. Sci. U. S. A.* **2013**, *110*, 40−45.
(25) Zhang, H. C.; Liu, S.; Shen, X.; Chen, L. H.; Li, L.; Cui, T. J. Broadband amplification of spoof surface plasmon polaritons at microwave frequencies. *Laser & Photon. Rev.* **2015**, *9*, 83−90.
(26) Grgić, J.; Ott, J. R.; Wang, F.; Sigmund, O.; Jauho, A.; Mørk, J.; Asger Mortensen, N. Fundamental Limitations to Gain Enhancement in Periodic Media and Waveguides. *Phys. Rev. Lett.* **2012**, *108*, 183903.
(27) Yang, Y.; Shen, X.; Zhao, P.; Zhang, H. C.; Cui, T. J. Trapping surface plasmon polaritons on ultrathin corrugated metallic strips in microwave frequencies. *Opt. Express* **2015**, *23*, 7031−7037.
(28) See Supporting Information for detailed descriptions. This material is available free of charge via the Internet at http://pubs.acs.org.
(29) Ma, H. F.; Shen, X.; Cheng, Q.; Jiang, W. X.; Cui, T. J. Broadband and high-efficiency conversion from guided waves to spoof surface plasmon polaritons. *Laser & Photon. Rev.* **2014**, *8*, 146−151.
(30) Sun, S.; He, Q.; Xiao, S.; Xu, Q.; Li, X.; Zhou, L. Gradient-index meta-surfaces as a bridge linking propagating waves and surface waves. *Nat. Mater.* **2012**, *11*, 426−431.
(31) Gao, X.; Zhou, L.; Liao, Z.; Ma, H. F.; Cui, T. J. An ultra-wideband surface plasmonic filter in microwave frequencies. *Appl. Phys. Lett.* **2014**, *104*, 191603.
(32) Yin, J. Y.; Ren, J.; Zhang, H. C.; Pan, B. C.; Cui, T. J. Broadband frequency-selective spoof surface plasmon polaritons on ultrathin metallic structure. *Sci. Rep.* **2015**, *5*, 8165.
(33) Manjavacas, A.; García de Abajo, F. J. Robust plasmon waveguides in strongly interacting nanowire arrays. *Nano Lett.* **2009**, *9*, 1285−1289.
(34) Manjavacas, A.; García de Abajo, F. J. Coupling of gap plasmons in multi-wire waveguides. *Opt. Express* **2009**, *17*, 19401−19413.
(35) Cai, W.; Wang, L.; Zhang, X.; Xu, J.; Garcia de Abajo, F. J. Controllable excitation of gap plasmons by electron beams in metallic nanowire pairs. *Phys. Rev. B: Condens. Matter Mater. Phys.* **2010**, *82*, 125454.
(36) Myroshnychenko, V.; Stefanski, A.; Manjavacas, A.; Kafesaki, M.; Merino, R. I.; Orera, V. M.; Pawlak, D. A.; García de Abajo, F. J. Interacting plasmon and phonon polaritons in aligned nano- and microwires. *Opt. Express* **2012**, *20*, 10879−10887.
(37) Haus, H. A.; Huang, W. Coupled mode theory. *Proc. IEEE* **1991**, *79*, 1505−1518.
(38) Ma, A.; Li, Y.; Zhang, X. Coupled mode theory for surface plasmon polariton waveguides. *Plasmonics* **2013**, *8*, 769−777.

DOI: 10.1021/acsphotonics.5b00316
ACS Photonics 2015, 2, 1333−1340